Journal of Zhejiang University-SCIENCE A (Applied Physics & Engineering) 2025 26(1):36-49
www.jzus.zju.edu.cn; www.springer.com/journal/11582
E-mail: jzus_a@zju.edu.cn

Research Articles

https://doi.org/10.1631/jzus.A2300590

Expansion mechanism of sulfate attack on cement-treated aggregates under freeze–thaw cycles

Qi WANG[1], Jiankun LIU[2,4]✉, Xu LI[3], Pengcheng WANG[5], Jingyu LIU[5], Mingzhi SUN[1]

[1]*Research Institute of Highway Ministry of Transport, Beijing 100088, China*
[2]*School of Civil Engineering, Sun Yat-sen University, Guangzhou 510006, China*
[3]*School of Civil Engineering, Beijing Jiaotong University, Beijing 100044, China*
[4]*State Key Laboratory for Tunnel Engineering, Guangzhou 510275, China*
[5]*Railway Engineering Research Institute, China Academy of Railway Sciences Corporation Limited, Beijing 100081, China*

Abstract: Sulfate attack-induced expansion of cement-treated aggregates in seasonally frozen regions is a well-known issue which causes continuous expansion in railway subgrades, and particularly in high-speed railways. Accordingly, we investigated the influence of material proportions, the number of freeze–thaw (FT) cycles, and temperature gradients on the expansion mechanism of sulfate attack on cement-treated aggregates subjected to FT cycles. The conditions, laws, and dominant factors causing the expansion of aggregates were analyzed through swelling tests. The results indicate that under FT cycles, 3% content cement-treated graded macadam only experiences slight deformation. The maximum strain of graded macadam attacked by 1% sodium sulfate content in each FT cycle is significantly larger than that of 3% content cement-treated graded macadam attacked by 1% sodium sulfate content. Using scanning electron microscopy, needle-like crystals were observed during sulfate attack of cement-treated graded macadam. Through quantitative analysis, we determined the recoverable and unrecoverable deformations of graded macadam under FT cycles. For graded macadam under sulfate attack, the expansion is mainly induced by periodic frost heave and salt expansion, as well as salt migration. For cement-treated graded macadam under sulfate attack, the expansion is mainly induced by chemical attack and salt migration. This study can serve as a reference for future research on the mechanics of sulfate attack on cement-treated aggregates that experience FT cycles, and provide theoretical support for methods that remediate the expansion induced by sulfate attack.

Key words: Sulfate attack; Freeze–thaw (FT) cycle; Expansion; Cement-treated aggregates; Dominant factors

1 Introduction

Sulfate attack is one of the main factors that causes damage to cement-treated subgrade fillings. Sherwood (1962) found that the formation of ettringite ($3CaO\cdot Al_2O_3\cdot 3CaSO_4\cdot 32H_2O$) and thaumasite was the main reason for sulfate attack cement-treated aggregates. Ettringite minerals, as they experience crystal growth, contribute to a large amount of heaving in soils (Puppala et al., 2019). The phenomena of cracking, heaving, loosening, peeling-off, developing a white pulpy appearance, and dissolution of cement paste have been observed in many railway subgrades and concrete structures for highways (Slater et al., 2003; Wang et al., 2003; Zhou et al., 2006; Alonso and Ramon, 2013; Wang et al., 2020). Sulfate attack on cement-treated materials may result in the formation of ettringite or gypsum within days or over decades (Wang et al., 2021).

In cold regions such as Northwest China, where the temperature is regularly below 0 °C in winter, geomaterials (e.g. cement-treated aggregates) are subjected to repeated freeze–thaw (FT) cycles as the seasons and temperatures change (Liu et al., 2015, 2022; Chang et al., 2022; Chen et al., 2024). Meanwhile, there are also many areas with saline soils, containing abundant sulfate ions (Wang et al., 2020). Thus, the cement-treated aggregates of ballastless track subgrades for high-speed railways are not only attacked by sulfates, but also damaged by FT cycles. Furthermore, the heave induced by FT cycles accelerates the formation of

✉ Jiankun LIU, liujiank@mail.sysu.edu.cn
Jiankun LIU, https://orcid.org/0000-0002-3064-8575

Received Nov. 20, 2023; Revision accepted Apr. 9, 2024;
Crosschecked Dec. 26, 2024

internal cracks in the cement-treated aggregates, which accelerates the diffusion of water and salt in aggregate, and exacerbates the sulfate attack reactions (Jiang et al., 2015). The expansion of cement-treated aggregates negatively impacts the normal operation of railways. Therefore, it is important to study the characteristics of expansion induced by sulfate attack in cement-treated aggregates that experience FT cycles.

Studies on the expansion mechanisms of cement-treated aggregates caused by sulfate attack and FT cycles can be divided into two categories. In one category, researchers investigate the changes in physical and mechanical properties of cement-treated aggregates as a result of sulfate attack and FT cycles, along with the associated chemical products. For instance, Xiao et al. (2019) discovered that as the number of FT cycles increases, ettringite and gypsum gradually form due to a reaction with sulfate in recycled concrete. Niu et al. (2013) also reported that ettringite and gypsum are the main corrosion products of concrete attacked by sulfate solutions and experiencing FT cycles. Furthermore, Chen et al. (2017) proposed that the longitudinal expansion of concrete is correlated with nonlinear parameters in sulfate attack and FT cycles. Additionally, Mardani-Aghabaglou et al. (2015) reported that the unconfined compressive strength of cement-treated clay decreased and its permeability increased under the combined effect of sulfate attack and FT cycles. In the other category of studies, the mechanism of sulfate attack on cement-treated aggregates experiencing FT cycles has been analyzed. For instance, Yao et al. (2023) conducted macroscopic physical-mechanical tests and microstructural characterization under the coupled action of sulfate attack and FT cycles, and a parabolic regression equation to predict recycled-powder concrete damage was established. Similarly, Xu et al. (2021) used experimental tests of the relative dynamic elastic modulus of recycled aggregate concrete experiencing sulfate attack and FT cycles, and accordingly established a Weibull distribution damage prediction model.

The expansion mechanism of sulfate attack on cement-treated aggregates experiencing FT cycles has been previously studied, and the understanding of this phenomenon is growing. However, it is worth noting that the studies of coupling effects between sulfate attack and FT cycles have only focused on the mechanical properties of fine particle-size materials. Few have studied the mechanism of sulfate attack on cement-treated graded macadam experiencing FT cycles, and limited damage models have been established for this scenario. Cement-treated graded macadam is a coarse particle filler with low water content and high compactness, so its properties are different and the dominant factors of expansion induced by sulfate attack and FT cycles have yet to be investigated.

Therefore, the objective of this study is to explore the expansion mechanism of sulfate attack on cement-treated aggregates under FT cycles. The proportions of materials, the number of FT cycles, and the temperature gradients are accordingly used as study variables. The conditions, laws, and dominant factors of expansion for cement-treated aggregates experiencing sulfate attack and FT cycles are accordingly investigated. The dominant factors of the expansion are quantitatively analyzed, considering the effects of sulfate chemical attack, salt migration, frost heave, and salt expansion. This study serves as a foundation for understanding the expansion mechanism of sulfate attack on cement-treated aggregates under FT cycles.

2 Materials and methods

2.1 Materials

In recent years, high-speed railways in Northwest China have experienced a continuous and severe heave. Field deformation and temperature of the subgrade were monitored between April 2017 and April 2018. The monitoring results showed that the ground temperature of the expansion site ranged from −10 to 30 ℃. The maximum expansion of the subgrade was approximately 69.5 mm. The surface of the subgrade bed was filled with compacted graded aggregate, which was treated with 3% content of Ordinary Portland cement (OPC). The SO_4^{2-} content on the top of the subgrade was close to 0.3%. Some expansive minerals (e.g., ettringite, thaumasite, and gypsum) were observed on the surface of the subgrade bed, indicating that the subgrade expansion is mainly caused by sulfate attack on cement-treated subgrade filler (Yao et al., 2019; Wang et al., 2020). Using screening tests according to the Code for Soil Test of Railway Engineering (MR, 2010), the particle size distribution on the surface layer of the subgrade bed was determined as shown in Fig. 1.

Two particle sizes of fresh aggregates were used in this study. To accurately simulate the field conditions,

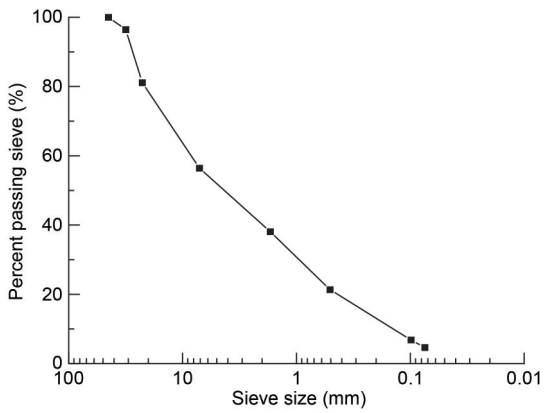

Fig. 1 Screen test of graded macadam of the surface layer of the subgrade bed

graded macadam with a particle size ranging from 0 to 16 mm is used. The particle size distribution of graded macadam used is consistent with that of the surface layer of the subgrade bed (Fig. 1). To compare the deformation law between graded macadam and fine aggregates under sulfate attack and FT cycles, stone powders with a particle size of less than 2 mm were also used. Based on the heavy compaction test (MR, 2010), the moisture–density curves of graded macadam and stone powders were obtained (Fig. 2). The optimum moisture content and maximum dry density of the stone powders were 11.2% and 2.36 g/cm^3, respectively. In the moisture–density curves of graded macadam, the minimum dry density was 2.25 g/cm^3, and the corresponding moisture content was 5.5%.

The samples mainly consist of aggregate, cement, sodium sulfate, and distilled water. OPC 42.5 was used in the tests, which mainly contains tricalcium silicate (34%), brownmillerite (15%), dicalcium silicate (11%), and tricalcium aluminate (7%). The cement contents were set to 3% to remain consistent with the condition of the surface bed. Considering that the sulfate content was close to 0.3% in the field reactions, and that we use sodium sulfate as the reactant to provide sulfate ions, we set the sulfate content to 1% to ensure an abundance of sulfate ions for the reactions. In view of how the active temperature for sulfate attack reactions was between 0 and 20 °C (Wang et al., 2020), and how the maximum temperature in the field was 28 °C, the thawing temperature was set to 30 °C. Considering that the minimum temperature in the field was –10 °C, the freezing temperatures of the two grades were set as −10 and −5 °C, respectively.

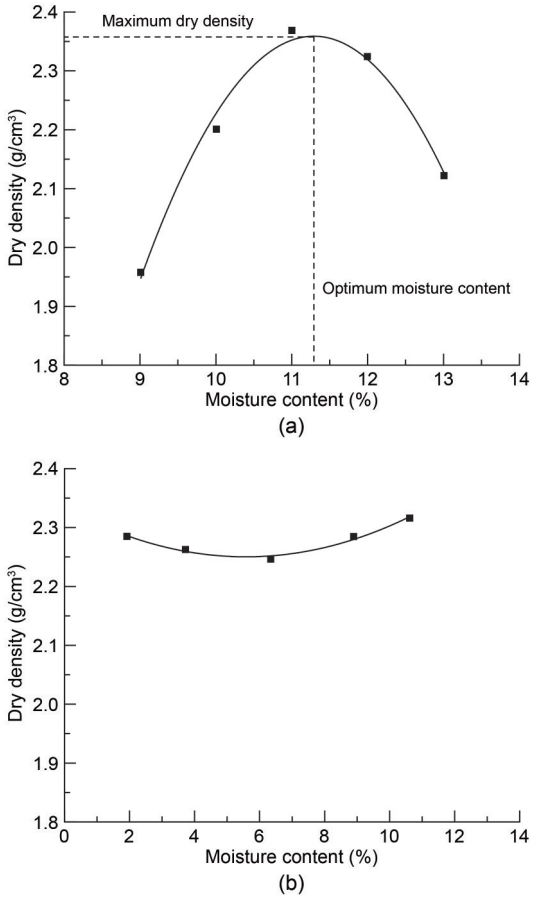

Fig. 2 Moisture–density curves of materials: (a) moisture–density curves of stone powders; (b) moisture–density curves of graded macadam

Three types of aggregates with different material ratios were considered in this study. The first type of aggregate contains 1% sodium sulfate, and its purpose is to explore the effects of salt expansion, frost heave, and salt migration. The second type of aggregate has 3% cement, and it is used to investigate the effect of frost heave and cement solidification. The third type of aggregate has 1% sodium sulfate and 3% cement, and it is used to analyze the coupling effects of frost heave, salt expansion, salt migration, cement solidification, and (sulfate) chemical attack.

2.2 Experimental procedures

Referring to the code (MR, 2010) and accounting for the aggregates' sizes, we consider two types of samples with different compositions and sizes in this study. The first is mainly composed of stone powders, and its sample size was 61.8 mm in diameter and 40 mm in height. The second is mainly composed of

graded macadam, and its sample size was 250 mm in diameter and 500 mm in height. There were also two different types of sample molds. One was a metal ring mold with a 61.8 mm inner diameter and 40 mm height, and the other was a perspex cylinder with a 250 mm inner diameter and a 500 mm height. To prevent the cracking of the plexiglass cylinder during the experiment, the cylinder was affixed with metal strips every 40 to 60 mm. In graded macadam swelling tests, the amounts of graded macadam, cement, sodium sulfate, and deionized water were calculated based on the dry density of 2.25 g/cm^3 and the moisture content of 5.5%. In stone powers swelling tests, the amounts of materials above were calculated based on the dry density of 2.36 g/cm^3 and the moisture content of 11.2%. The calculation of material amounts and the material mixing process were performed in accordance with the code (MR, 2010).

For the graded macadam swelling test, first, the temperature of the test chamber was set to the test values. Then, the aggregates were stirred with sodium sulfate. Subsequently, deionized water was added to the mixture and stirred. Then the mixture was stirred with cement until it was homogeneous. Next, the materials were compacted into the perspex cylinder mold. Considering the larger size of the graded macadam samples, the compaction of the mixture was divided into five layers. At the later stage of the 5th compacted layer, an electric drill was used to drill a small hole into the sample at every 100 mm of height, and a temperature sensor was inserted into the graded macadam. The compaction was continued until the sample was at 500 mm height. The sample with temperature sensors was wrapped with an impermeable plastic film, and then put into the test chamber (with a set temperature and humidity). A perspex sheet was placed on top of the sample. The electronic dial gauge was affixed by a metal stent, and the needle tip of the dial gauge was in vertical contact with the middle part of the perspex sheet's surface. At last, the electronic dial gauge was connected to the computer through a displacement data acquisition instrument. The temperature data was recorded each minute and the displacement data was recorded every 5 min. Fig. 3 shows the procedure for the graded macadam swelling tests. Fig. 4 shows the details of the sulfate attack swelling tests. For the stone powder samples with small particle size, the materials were compacted into the metal ring only at one time, and the temperature was not monitored. Furthermore, in the graded macadam swelling test, the plexiglass sheet was replaced with porous stone (Fig. 5). After 30 d, small cubic samples were taken from the center of the complete samples, with dimensions of 1.5 cm× 1.5 cm×1.0 cm, in preparation for scanning electron microscope (SEM) tests. The Hitachi S-4800 SEM system was used to perform the measurements.

In this study, the strain of the sample was calculated using the value of vertical swelling (ΔH) and the initial height of the sample (H_0) as shown in Eq. (1):

$$\varepsilon = \frac{\Delta H}{H_0} \times 100\%. \tag{1}$$

In each FT cycle, the samples first experienced different freezing temperatures of −10 ℃ (for 72 h) or −5 ℃ (for 36 h), and then thawing temperatures of 30 ℃ (for 72 or 36 h). This FT cycle was repeated five and ten times, respectively. Temperature and displacement measurements of the samples were performed for 30 d. For this experiment, the sample preparation

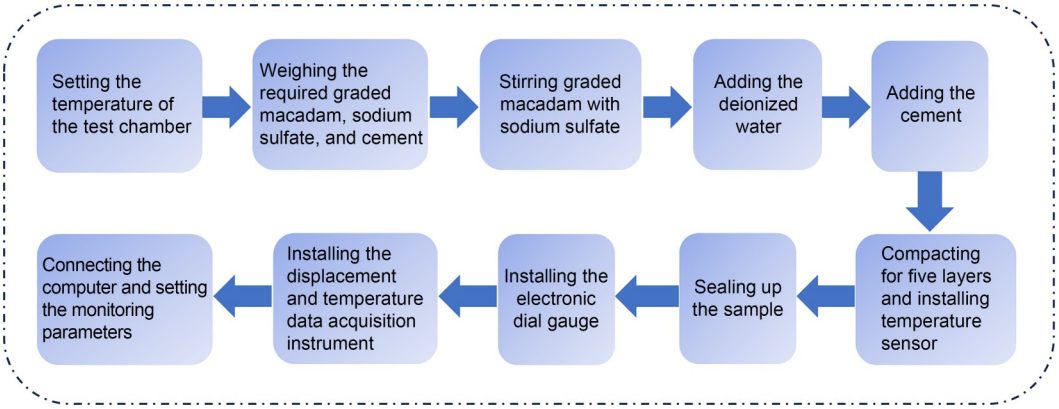

Fig. 3 Flow chart of the graded macadam swelling test

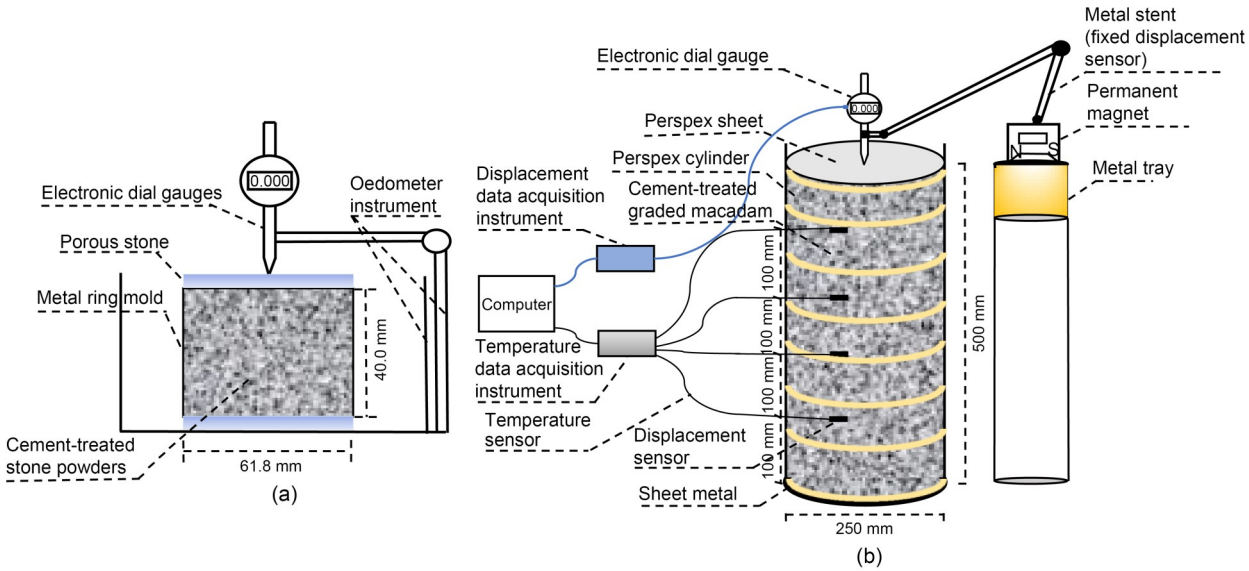

Fig. 4 Details for swelling tests of sulfate attack (unit: mm): (a) swelling test device for stone powder samples; (b) swelling test device for graded macadam samples

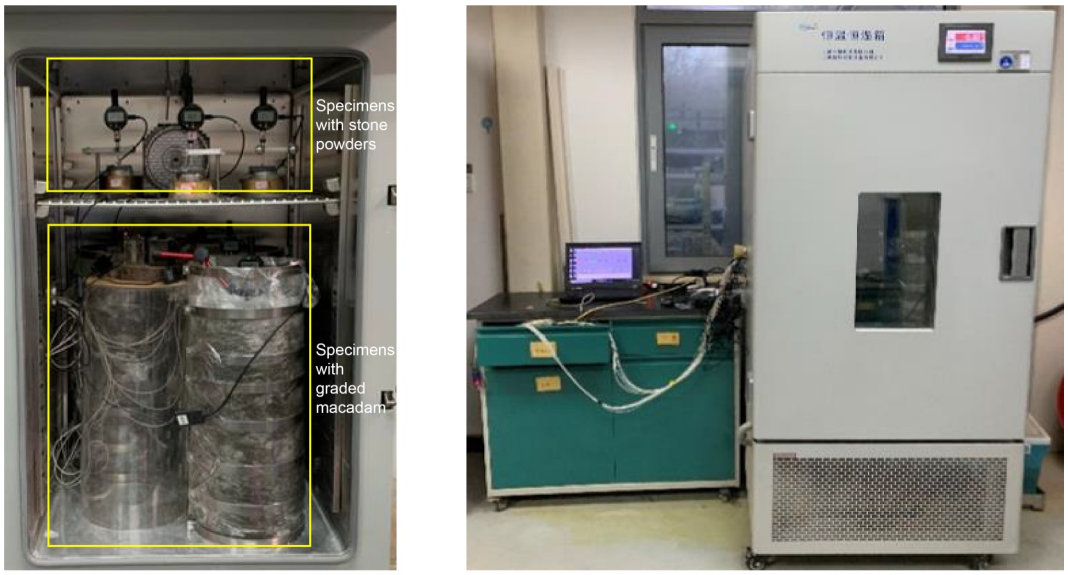

Fig. 5 Swelling tests of sulfate attack: (a) samples before the test; (b) swelling test device

matrix, aggregate size, sample size, and FT cycle conditions are shown in Table 1.

3 Results

3.1 Expansion induced by sulfate attack for temperatures between −10 and 30 ℃

Fig. 6 illustrates the temperature monitoring result of −10 ℃-G-1%S-3%C. The temperatures of four locations inside the sample (100, 200, 300, and 400 mm) reached the expected temperature within about 32 h during each FT cycle. The maximum temperature reached was approximately 30 ℃, and the minimum temperature was about −10 ℃.

It can be seen in Fig. 7 that the strains changed periodically with the periodic changes of temperature within the samples. During the freezing period in the 5th FT cycle, the maximum strains of −10 ℃-G-1%S, −10 ℃-G-1%S-3%C, −10 ℃-B-1%S, and −10 ℃-B-1%S-3%C

Table 1 Sample preparation matrix under FT cycle conditions

Time of each freezing/ thawing (h)	Number of FT cycles	Freezing/thawing temperature (℃)	Aggregate	Diameter (mm)	Height (mm)	Sodium sulfate content (%)	Cement content (%)	Designation
72/72	5	−10/30	Graded macadam	250.0	500	1	3	−10 ℃-G-1%S-3%C
						1	0	−10 ℃-G-1%S
			Stone powders	61.8	40	1	3	−10 ℃-B-1%S-3%C
						1	0	−10 ℃-B-1%S
36/36	10	−5/30	Graded macadam	250.0	500	1	3	−5 ℃-G-1%S-3%C
						1	0	−5 ℃-G-1%S
						0	3	−5 ℃-G-3%C
			Stone powders	61.8	40	1	3	−5 ℃-B-1%S-3%C
						1	0	−5 ℃-B-1%S
						0	3	−5 ℃-B-3%C

G presents the graded macadam, B presents the stone powders, S presents the sodium sulfate, and C presents the cement

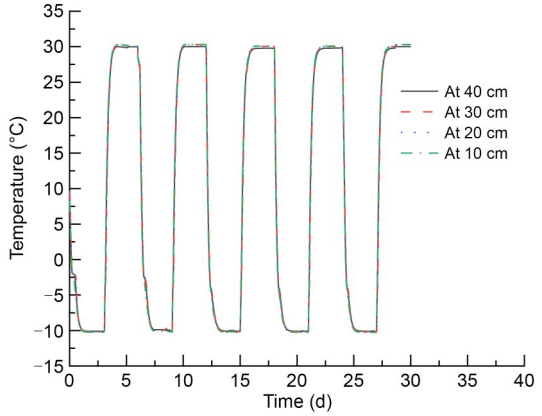

Fig. 6 Temperature monitoring results of −10 ℃-G-1%S-3%C

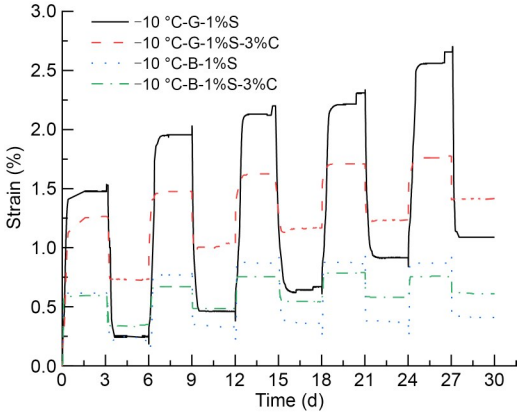

Fig. 7 Strain curves of samples over time under temperatures between −10 and 30 ℃

were approximately 2.70%, 1.78%, 0.87%, and 0.76%, respectively. Compared with stone powder samples, the graded macadam samples took a longer time to reach the strain stabilization stage. This is because of the larger volume of the graded macadam samples, making it take a longer time for the internal temperatures to reach the expected values.

For the same sample size, both the maximum and minimum strains for the samples with only sodium sulfate (−10 ℃-G-1%S and −10 ℃-B-1%S) were significantly greater than those of the samples with sodium sulfate and cement (−10 ℃-G-1%S-3%C and −10 ℃-B-1%S-3%C) for each FT cycle. During the temperature change, the amplitudes of strain change for the samples with cement (−10 ℃-G-1%S-3%C and −10 ℃-B-1%S-3%C) were smaller than those of the samples without cement (−10 ℃-G-1%S and −10 ℃-B-1%S).

When the temperature decreased to the freezing temperature, the water in the pores was frozen. Water in the unfrozen area then migrated and accumulated in the frozen area, eventually forming ice crystals. This led to an increase in crystal volume and an increase in the distance between particles, resulting in the expansion of samples (Qiu et al., 1994). The ice crystals then melted due to the subsequent temperature increase, which caused a decrease in the volume of the samples. Therefore, the strain of the aggregates increased and decreased periodically along with the periodic FT cycles.

For graded macadam samples, the maximum and minimum values of strain in each FT cycle were greater than those of the previous cycle, for five FT cycles. Compared with the 4th FT cycle, the maximum value of strain for −10 ℃-G-1%S (without cement) still

increased significantly in the 5th FT cycle, while the maximum strain of −10 ℃-G-1%S-3%C (with cement) increased slowly. Due to the periodic frost heave and salt expansion, the expansion of −10 ℃-G-1%S continuously increased, and cracks inside the samples expanded. This was conducive to salt migration and fracture development. For −10 ℃-G-1%S-3%C, in addition to the effects of salt migration and crystallization, frost heave, and cement hydration, the chemical attack reactions also played an important role in expansion (Santhanam et al., 2003; Puppala et al., 2005; Ren and Lai, 2021). With the increase of reaction time and the consumption of reactants, the rate of formation of expansion minerals decreased, leading to the strain in the aggregates increasing slowly. Furthermore, water and sodium sulfate were consumed in the process of sulfate attack on cement-treated aggregate, and thus the expansion induced by ice and salt crystals was reduced. The maximum strain of stone powder samples (−10 ℃-B-1%S-3%C and −10 ℃-B-1%S) within a cycle increased for three FT cycles, and then essentially remained stable. This may be due to the small particle size of the stone powder, which caused the relatively small degree of particle fragmentation under the FT cycles and sulfate attacks.

3.2 Expansion induced by sulfate attack under temperatures between −5 and 30 ℃

Through the temperature monitoring results, the temperatures of four locations in the sample reached the expected temperature within each FT cycle. The maximum temperature reached was about 30 ℃, and the minimum temperature reached was about −5 ℃.

As shown in Fig. 8, the strains changed periodically along with the periodic changes of the temperature. For the same sample size, the strain of the samples with 3% cement content (−5 ℃-G-3%C or −5 ℃-B-3%C) was the smallest. The strains of the samples with 3% cement content and 1% sodium sulfate content (−5 ℃-G-1%S-3%C or −5 ℃-B-1%S-3%C) were larger than the samples with only 3% cement content. The strain of the samples with only 1% sodium sulfate content (−5 ℃-G-1%S or −5 ℃-B-1%S) was the largest.

We can also see in Fig. 8 that the maximum and minimum strains of −5 ℃-G-1%S (or −5 ℃-B-1%S) within each FT cycle increased as the number of FT cycles increased. These strains were also greater than

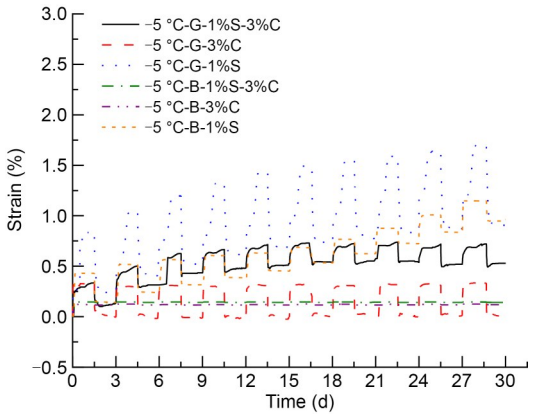

Fig. 8 Strain curves of samples over time under temperature between −5 and 30 ℃

that of −5 ℃-G-3%C (or −5 ℃-B-3%C) in each cycle. The maximum strains of −5 ℃-G-1%S reached 0.84% during the first FT cycle, then reached 1.70% during the 10th FT cycle. Compared to the previous cycle, the maximum and minimum strains of −5 ℃-G-3%C essentially remained stable. Within six FT cycles, the maximum and minimum strains of −5 ℃-G-1%S-3%C increased as the number of FT cycles increased. These strains reached 0.72% and 0.51%, respectively, at the 6th FT cycle, and subsequently remained almost stable as the FT cycles increased. Within 30 d, the maximum strain of −5 ℃-B-1%S within each FT cycle increased from 0.43% (the first FT cycle) to 1.15% (the 10th FT cycle). Compared with −5 ℃-B-1%S, the strains of −5 ℃-B-3%C and −5 ℃-B-1%S-3%C were smaller, though both of them still experienced periodic deformation. The strain of −5 ℃-B-3%C fluctuated between 0.12% and 0.13%, and the strain of −5 ℃-B-1%S-3%C fluctuated between 0.14% and 0.15%. In contrast to the larger strain of −5 ℃-B-1%S, the smaller strains of −5 ℃-B-3%C and −5 ℃-B-1%S-3%C exemplified the solidification effect of the cement, inhibiting the expansion of the sample.

3.3 Analysis of strains under two temperature gradients

Fig. 9 compares the strain of graded macadam with 1% sodium sulfate for two different temperature gradients. Within 30 d, −10 ℃-G-1%S experienced five FT cycles. The maximum and minimum strains in each cycle increased as the number of FT cycles increased. Within 30 d, −5 ℃-G-1%S experienced 10 FT cycles. After seven FT cycles, the rate of increase of the

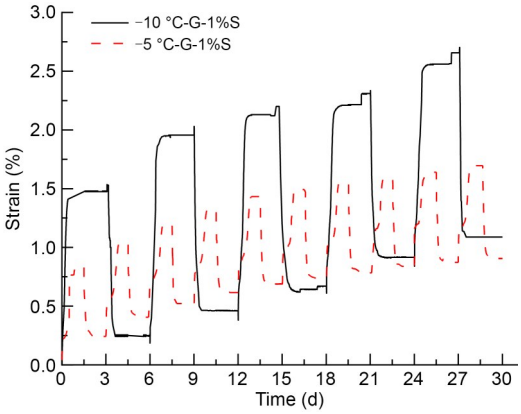

Fig. 9 Strains of graded macadam attacked by sodium sulfate under different temperature gradients

maximum and minimum strains in each FT cycle decreased as the number of cycles increased. For the same FT cycles, the maximum and minimum strains of −10 °C-G-1%S were greater than those of −5 °C-G-1%S. After five FT cycles, the strain of −10 °C-G-1%S (on the 30th day) was greater than that of −5 °C-G-1%S (on the 15th day). Under the greater temperature variability, the salt migration was more violent, which resulted in more cracking in the samples, as well as greater expansion of the aggregate.

Fig. 10 compares the strain of graded macadam with 1% sodium sulfate content and 3% cement content for two different temperature gradients. The strain of −10 °C-G-1%S-3%C was significantly greater than that of −5 °C-G-1%S-3%C. The maximum and minimum strains of −10 °C-G-1%S-3%C increased with the number of FT cycles, increasing rapidly in the first three FT cycles, and thereafter increasing slowly. Within 30 d, −5 °C-G-1%S-3%C experienced 10 FT cycles.

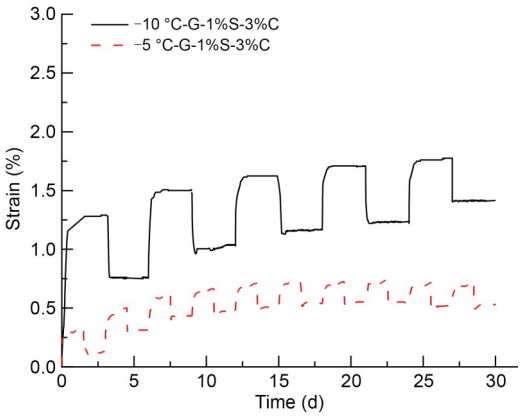

Fig. 10 Strains of cement-treated graded macadam attacked by sodium sulfate under different temperature gradients

This sample exhibited similar strain tendencies as −10 °C-G-1%S-3%C in the first five FT cycles. Then, the maximum and minimum strains of −5 °C-G-1%S-3%C essentially remained stable as the number of FT cycles increased.

The expansions of −10 °C-G-1%S-3%C and −5 °C-G-1%S-3%C were not only induced by salt expansion, frost heave, and salt migration, but were also influenced by sulfate chemical attack. Due to the greater temperature range of −10 to 30 °C compared to −5 to 30 °C, the salt migration in −10 °C-G-1%S-3%C was more violent, leading to more cracks being generated. Thus, the loose structure of aggregates was also conducive to the transport of reactant ions within the pore solution under thawing temperatures, which resulted in more intense sulfate attack and more severe expansion.

4 Discussion

Expansion due to sulfate attack under FT cycles can be considered as either recoverable deformation or unrecoverable expansion. With the periodic change of temperature, the recoverable deformation presents a periodic increase or decrease, returning to normal, while the unrecoverable expansion does not. We examine these two cases in detail in the subsequent sections.

4.1 Analysis of recoverable deformation

Recoverable deformation is mainly induced by frost heave and salt expansion. At freezing temperatures, the expansion of −5 °C-G-3%C increased, which was caused by water freezing into ice crystals in the pore space. At thawing temperatures, the ice melting into water led to the strain of −5 °C-G-3%C decreasing.

For aggregates with sodium sulfate, the expansion of the sample was not only induced by frost heave but also affected by salt expansion. Because we used temperatures ranging from −10 to 30 °C and −5 to 30 °C in this study, the mirabilite can be considered as the only product of sodium sulfate crystallization (Flatt, 2002; Thaulow and Sahu, 2004; Gao, 2010). Comparing our results with the phase diagram of sodium sulfate crystallization (Gao, 2010), the sodium sulfate solution in the pores was almost saturated at about 7 °C. As the temperature decreased, the solubility of sodium sulfate in the pores decreased continuously. This combined with the free water and weakly-bound

water in the pores resulted in the continuous formation of mirabilite crystals. At freezing temperatures (−5 or −10 ℃), the formation of mirabilite crystals and ice crystals had a positive influence on the development of cracks and the expansion of samples. As the temperature increased, the solubility of sodium sulfate in the pores increased and mirabilite crystals dissolved, causing the deformation of −10 ℃-G-1%S to decrease.

4.2 Analysis of unrecoverable expansion

Unrecoverable expansion is mainly caused by the products of chemical attack and salt migration. During the FT cycles, the unrecoverable expansion of −10 ℃-G-1%S and −5 ℃-G-1%S were mainly induced by salt migration. At thawing temperatures, as water was evaporating, salt migrated upwards and continuously accumulated with the water, which resulted in the aggregation of sulfate at the top of the sample, and led to loosening and expansion.

Salt migration causes salt accumulation and precipitation at freezing temperatures, a process which cannot completely reverse at thawing temperatures (Chen et al., 2006). This means that during each FT cycle, there is an unrecoverable part of the expansion induced by the salt migration. During decreases in temperature, the formation of mirabilite and ice caused the expansion of the samples. Therefore, under FT cycles, the freezing and melting of water, in addition to the effects of the mirabilite crystallization and dissolution, caused the expansion and shrinking of the samples. The structure of the samples was damaged by these repeated processes of expansion and shrinking, which also accelerated the salt migration.

For aggregates with sodium sulfate and cement, sulfate reacting with cement hydration products resulted in severe expansion (Jiang et al., 2015). From the SEM images of −5 ℃-G-1%S-3%C, it can be seen that a large number of needle-like minerals (of size 2–5 μm) were generated (Fig. 11). Under FT cycles, the expansions of −10 ℃-G-1%S-3%C and −5 ℃-G-1%S-3%C were not only induced by the formation of mirabilite crystals and ice crystals, but also caused by salt migration and generation of needle-like crystals from chemical attack. We make the reasonable assumptions that ettringite and gypsum crystals are the products of sulfate chemical attack, and the expansion induced by ettringite and gypsum is unrecoverable. Additionally,

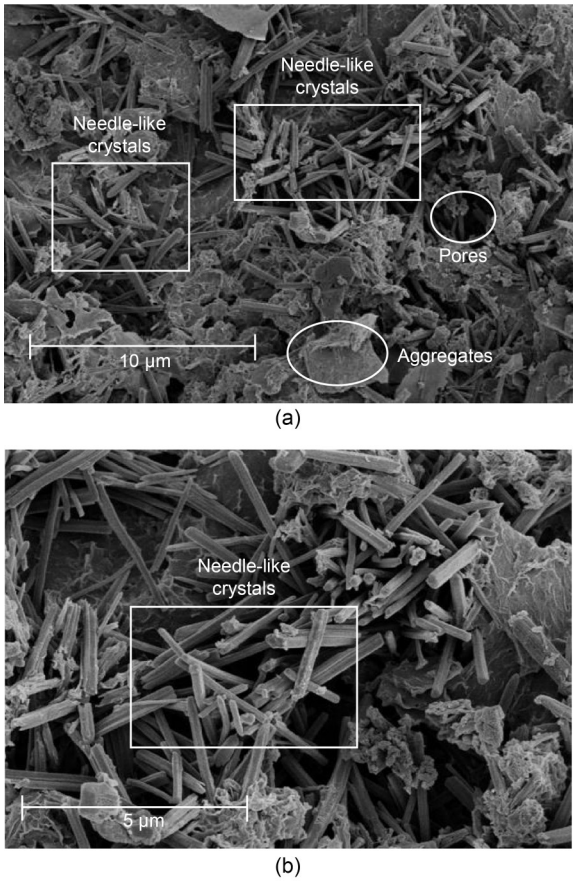

Fig. 11 SEM images of (a) −5 ℃-G-1%S-3%C and (b) enlarged image of needle-like crystals

we assume gypsum is generated by the reaction between calcium hydroxide (the hydration product of tricalcium silicate) and sodium sulfate, and ettringite is generated by the reaction between tricalcium aluminate and gypsum. Thus, 1 mol of ettringite ($3CaO·Al_2O_3·3CaSO_4·32H_2O$) being generated consumes at least 1 mol of tricalcium aluminate ($3CaO·Al_2O_3$), 3 mol of sodium sulfate (Na_2SO_4), 2 mol of tricalcium silicate ($3CaO·SiO_2$), and 32 mol of water (H_2O). The chemical formation of ettringite has been shown in Eqs. (2)–(4). Thus, 1 mol of ettringite being generated theoretically consumes sodium sulfate, water, tricalcium aluminate, and tricalcium silicate in the mass proportions of 1.6∶2.1∶1.0∶1.7.

The cement used in this study contains 7% tricalcium aluminate and 34% tricalcium silicate. For −10 ℃-G-1%S-3%C and −5 ℃-G-1%S-3%C, the mass fraction of tricalcium aluminate for the total reactants is 0.21%, which was much smaller than that of tricalcium silicate, sodium sulfate, and water. Therefore,

the amount of tricalcium aluminate determined the end of the chemical attack reaction.

$$2(3CaO\cdot SiO_2)+6H_2O\rightarrow 3CaO\cdot 2SiO_2\cdot 3H_2O+3Ca(OH)_2, \quad (2)$$

$$Na_2SO_4+Ca(OH)_2+2H_2O\rightarrow CaSO_4\cdot 2H_2O+2NaOH, \quad (3)$$

$$3CaO\cdot Al_2O_3+3(CaSO_4\cdot 2H_2O)+26H_2O\rightarrow 3CaO\cdot Al_2O_3\cdot 3CaSO_4\cdot 32H_2O\ (\text{ettringite}). \quad (4)$$

The molar mass of gypsum is 172 g/mol. Thus, generating 1 mol of gypsum theoretically consumes tricalcium silicate and sodium sulfate in the molar proportion of 2:3 (in terms of mass proportion of 3.1:2.5). Therefore, generating 1 mol of gypsum theoretically consumes cement and sodium sulfate in the mass ratio of 3.73:1.00. The mass ratio of cement to sodium sulfate is about 3:1 for our case. This means if gypsum is considered the only product of the chemical attack, then the amount of sodium sulfate was excessive, and the amount of cement controlled the end of the reaction.

Therefore, whether ettringite or gypsum was regarded as the only product, our analysis indicates that the amount of sodium sulfate was sufficient, and the end of the chemical reaction was controlled by the amount of cement.

4.3 Analysis of dominant factors

During FT cycles, the deformation of samples with 1% sodium sulfate content (−10 ℃-G-1%S and −5 ℃-G-1%S) was mainly caused by periodic frost heave and salt expansion, and salt migration. We assume that the deformation induced by periodic frost heave and salt expansion is recoverable, and the deformation caused by salt migration is unrecoverable. The expansion of samples with 1% sodium sulfate content and 3% cement content (−10 ℃-G-1%S-3%C and −5 ℃-G-1%S-3%C) was not only induced by the above factors, but also affected by chemical attack. The deformation induced by chemical attack is assumed to be an unrecoverable expansion.

Fig. 12 shows strain curves of samples over time for the *N*th FT cycle. The formulas for calculating the recoverable strain ε_r and unrecoverable strain ε_{ur} after the *N*th FT cycle are respectively shown in Eqs. (5) and (6):

$$\varepsilon_r=\varepsilon_{Max}-\varepsilon_{Min}, \quad (5)$$

$$\varepsilon_{ur}=\varepsilon_{Min}, \quad (6)$$

where ε_{Max} and ε_{Min} represent the maximum and minimum strains in the *N*th FT cycle, respectively.

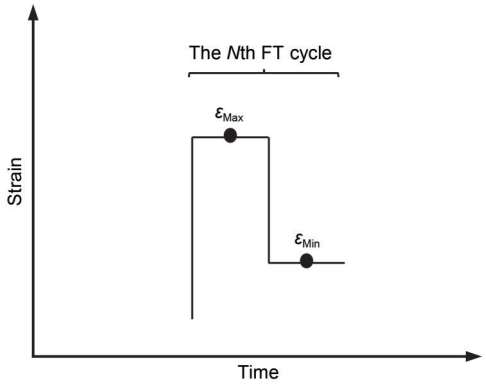

Fig. 12 Strain curves of samples over time in the *N*th FT cycle

Using the results from Figs. 7 and 8, the recoverable and unrecoverable strains of −5 ℃-G-3%C, −10 ℃-G-1%S, −5 ℃-G-1%S, −10 ℃-G-1%S-3%C, and −5 ℃-G-1%S-3%C are shown in Figs. 13–15.

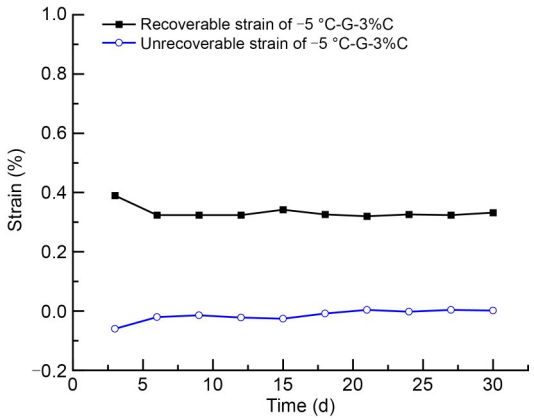

Fig. 13 Recoverable and unrecoverable strains of −5 ℃-G-3%C

4.3.1 Analysis of expansion behavior of −5 ℃-G-3%C

Fig. 13 illustrates the recoverable and unrecoverable strains of −5 ℃-G-3%C. It is clear that the unrecoverable strain was almost maintained at zero, and the recoverable strain was also small. This indicates that FT cycles have little effect on the development of cracks in −5 ℃-G-3%C, and that only slight deformation was induced by the freezing of water and melting of ice.

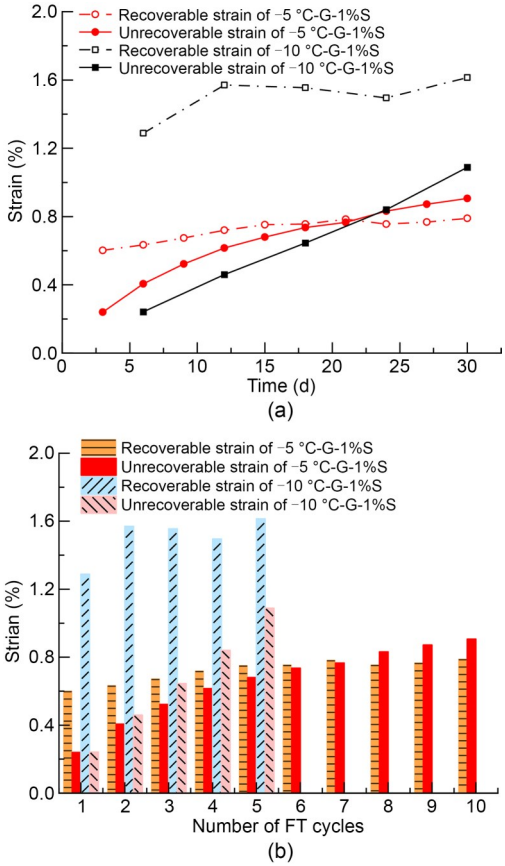

Fig. 14 Recoverable and unrecoverable strains of −5 °C-G-1%S and −10 °C-G-1%S: (a) recoverable and unrecoverable strains curves over time; (b) recoverable and unrecoverable strain histogram over the number of FT cycles

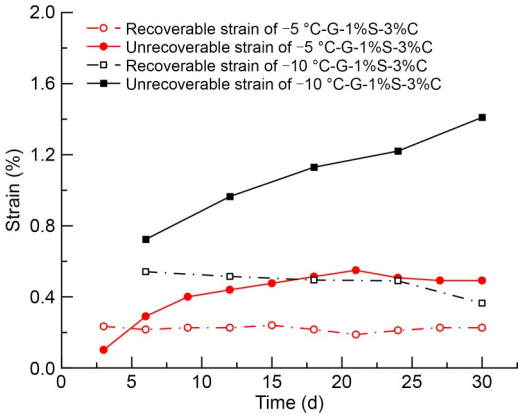

Fig. 15 Recoverable and unrecoverable strains of −5 °C-G-1%S-3%C and −10 °C-G-1%S-3%C

4.3.2 Analysis of expansion behaviors of −10 °C-G-1%S and −5 °C-G-1%S

Fig. 14a illustrates the recoverable and unrecoverable strains of −10 °C-G-1%S and −5 °C-G-1%S. At temperatures between −10 and 30 °C, −10 °C-G-1%S experienced five FT cycles within 30 d, and the recoverable strain was significantly greater than the unrecoverable strain. Furthermore, the unrecoverable strain of −10 °C-G-1%S increased almost linearly. At temperatures between −5 and 30 °C, −5 °C-G-1%S experienced 10 FT cycles within 30 d. It can be seen that the recoverable strain was larger than the unrecoverable strain within seven FT cycles. As the number of cycles increased, the unrecoverable strain increased rapidly, and the recoverable strain increased slowly. After seven FT cycles, the unrecoverable strain was larger than the recoverable strain in −5 °C-G-1%S.

From Fig. 14b, it can also be seen that the recoverable strain of −10 °C-G-1%S was significantly greater than that of −5 °C-G-1%S under the same FT cycles. The maximum recoverable strains of −10 °C-G-1%S and −5 °C-G-1%S were 1.61% (at the 5th cycle) and 0.79% (at the 10th cycle), respectively. The average values of recoverable strain for −10 °C-G-1%S and −5 °C-G-1%S were about 1.50% and 0.72%, respectively. The unrecoverable strain of −10 °C-G-1%S was close to that of −5 °C-G-1%S at the first FT cycle, being about 0.24%. At the 5th FT cycle, the unrecoverable strains of −10 °C-G-1%S and −5 °C-G-1%S were about 1.09% and 0.68%, respectively. At the 10th FT cycle, the unrecoverable strain of −5 °C-G-1%S was approximately 0.91%.

During the FT cycles, the expansions of −10 °C-G-1%S and −5 °C-G-1%S were mainly induced by the recoverable deformation of periodic salt expansion and frost heave, and the unrecoverable expansion of salt migration. As the number of FT cycles increased, the cracks in the sample expanded continuously. Moreover, due to the salt migration, the sample became loose and the unrecoverable strain increased continuously. This caused the unrecoverable strain of −5 °C-G-1%S to grow continuously and exceed the recoverable strain after seven FT cycles. Thus, the larger the temperature range experienced by the samples, the more intense the salt migration, and the more unrecoverable expansion. Therefore, for the same number of cycles, the unrecoverable strain of −10 °C-G-1%S was significantly greater than that of −5 °C-G-1%S.

Larger pores are more prone to phase transitions than smaller pores (Coussy, 2006; Xiao et al., 2018). Therefore, during FT cycles, the solutions in the larger pores freeze more easily than in the smaller pores.

Under the same cycles, more cracks were generated and more recoverable deformation occurred at the temperatures ranging from −10 to 30 ℃, which led to the larger pore size. Therefore, during cooling, the water in the pores was more amenable to phase transitions and was frozen into ice crystals, which caused more deformation in −10 ℃-G-1%S. Therefore, the recoverable strain of −10 ℃-G-1%S was significantly greater than that of −5 ℃-G-1%S. Thus, under the same FT cycles, both the recoverable strains and unrecoverable strains of −10 ℃-G-1%S were significantly greater than that of −5 ℃-G-1%S.

4.3.3 Analysis of expansion behaviors of −10 ℃-G-1%S-3%C and −5 ℃-G-1%S-3%C

From Fig. 15, it is clear that the unrecoverable strains of −10 ℃-G-1%S-3%C and −5 ℃-G-1%S-3%C were significantly greater than the recoverable strains on the whole. The average recoverable strain of −10 ℃-G-1%S-3%C (approximately 0.48%) was greater than that of −5 ℃-G-1%S-3%C (approximately 0.22%). The maximum value of unrecoverable strain of −10 ℃-G-1%S-3%C (approximately 1.41%, at the 5th FT cycle) was greater than that of −5 ℃-G-1%S-3%C (approximately 0.55%, at the 7th FT cycle).

For −10 ℃-G-1%S-3%C and −5 ℃-G-1%S-3%C, due to the chemical reactions between sulfate ions and cement hydration products, the products of chemical attack played an important role in the unrecoverable expansion. Therefore, the unrecoverable strains of −10 ℃-G-1%S-3%C and −5 ℃-G-1%S-3%C were in general significantly greater than the recoverable strains. Additionally, Fig. 15 illustrates that the unrecoverable strain of −10 ℃-G-1%S-3%C was significantly greater than that of −5 ℃-G-1%S-3%C. Essentially, the salt migration was more intense under the greater temperature range. This was conducive to the transportation of water and sulfate ions and promoted the chemical reactions, resulting in the greater unrecoverable deformation of −10 ℃-G-1%S-3%C. From Figs. 13–15, it also can be seen that for cement-treated aggregates experiencing sulfate attack, this chemical attack played a large role in the development of unrecoverable strain.

Table 2 summarizes the dominant factors of expansion induced by sulfate attack during FT cycles. For cement-treated graded macadam (−5 ℃-G-3%C), the sample only experienced slight recoverable deformation caused by periodic frost heave, and barely exhibited unrecoverable expansion. For sulfate attack on graded macadam (without cement, −5 ℃-G-1%S and −10 ℃-G-1%S), the deformation was mainly caused by both recoverable deformation and unrecoverable expansion. Additionally, the recoverable deformation caused by periodic frost heave and salt expansion accounted for about 43%–56% of the total deformation. Furthermore, the unrecoverable expansion caused by salt migration accounted for approximately 44%–57% of the total deformation. In the context of sulfate attack on cement-treated graded macadam (−5 ℃-G-1%S-3%C and −10 ℃-G-1%S-3%C), the expansion was dominated by unrecoverable expansion as caused by chemical attack and salt migration. In this case, the unrecoverable expansion accounted for about 70% of the total deformation.

5 Conclusions

In seasonally frozen regions, sulfate attack-induced expansion of cement-treated aggregates is a well-known problem causing heave in road and railway subgrades.

Table 2 Dominant factors of expansion induced by sulfate attack under FT cycles

Designation	Proportion of average recoverable strain to the maximum strain	Principal deformation	Dominant factor of expansion
−5 ℃-G-3%C	100%	Recoverable	Slight periodic frost heave
−5 ℃-G-1%S	43%	Recoverable and unrecoverable	Periodic frost heave and salt expansion, salt migration
−10 ℃-G-1%S	56%	Recoverable and unrecoverable	Periodic frost heave and salt expansion, salt migration
−5 ℃-G-1%S-3%C	31%	Unrecoverable	Chemical attack, salt migration
−10 ℃-G-1%S-3%C	27%	Unrecoverable	Chemical attack, salt migration

Cement-treated graded macadam as a coarse particle filler is widely used in road and railway subgrades, but its response to sulfate attack and FT cycles has not been investigated. Therefore, based on swelling tests of graded macadam experiencing sulfate attack during FT cycles, and quantitative analysis of the recoverable deformation and unrecoverable expansion, we determined the expansion characteristics and dominant influencing factors of sulfate attack.

We found that during FT cycles, the deformation of samples with 1% sulfate content was larger than for the samples with 1% sulfate and 3% cement content. The samples with 3% cement content only experienced slight deformation. Furthermore, the deformation of samples with 1% sulfate content (or with 1% sulfate content and 3% cement content) increased rapidly within the first seven FT cycles (or three FT cycles), and then increased slowly.

Under the same FT cycles, the lower the FT temperatures, the greater the recoverable and unrecoverable strains in samples with 1% sulfate content (or with 1% sulfate and 3% cement content). For samples with only 1% sulfate content, the unrecoverable strains are greater than the recoverable strains after seven FT cycles, while during initial cycles they are smaller than that of recoverable strains. For samples with 1% sulfate and 3% cement content, the unrecoverable strains are significantly greater than recoverable strains.

With regards to sulfate attack on aggregates (without cement), the expansion is mainly induced by periodic frost heave and salt expansion, as well as salt migration. Furthermore, about 44%–56% of the deformation was unrecoverable. For sulfate attack on cement-treated aggregates, the expansion is mainly induced by chemical attack and salt migration. In this case, about 70% of the deformation was unrecoverable. For sulfate attack on cement-treated aggregates, we also observed abundant needle-like crystals (of length 2–5 μm) through SEM tests.

In this study, the dominant factors of expansion induced by sulfate attack were investigated by measuring the recoverable deformation and unrecoverable expansion for different cases. We provide a new viewpoint for research on the mechanisms of sulfate attack. In summary, we find that expansion induced by sulfate attack is influenced by the coupled effects of frost heave, salt expansion, salt migration, and chemical reactions. In the future, the mechanism of expansion induced by sulfate attack could be studied more comprehensively, perhaps through multi-field-coupling numerical analysis.

Acknowledgments

This work is supported by the National Natural Science Foundation of China (Nos. 42171130 and 42301158), the Pilot Project of China's Strength in Transportation for the Central Research Institute (No. QG2021-1-4-7), and the National Key Technology Research and Development Program of the Ministry of Science and Technology of China (No. 2021YFB2601200).

Author contributions

Qi WANG, Jiankun LIU, and Xu LI designed the research and processed the corresponding data. Qi WANG wrote the first draft of the manuscript. Pengcheng WANG and Jingyu LIU helped to organize the manuscript. Mingzhi SUN revised and edited the final version.

Conflict of interest

Qi WANG, Jiankun LIU, Xu LI, Pengcheng WANG, Jingyu LIU, and Mingzhi SUN declare that they have no conflict of interest.

References

Alonso EE, Ramon A, 2013. Massive sulfate attack to cement-treated railway embankments. *Géotechnique*, 63(10):857-870. https://doi.org/10.1680/geot.sip13.p.023

Chang J, Liu JK, Li YL, 2022. Frozen sand–concrete interface direct shear behavior under constant normal load and constant normal height boundary. *Journal of Zhejiang University-SCIENCE A (Applied Physics & Engineering)*, 23(11):917-932. https://doi.org/10.1631/jzus.A2200118

Chen J, Bharata R, Yin TY, et al., 2017. Assessment of sulfate attack and freeze–thaw cycle damage of cement-based materials by a nonlinear acoustic technique. *Materials and Structures*, 50(2):105. https://doi.org/10.1617/s11527-016-0949-7

Chen QM, Ghimire B, Su LB, et al., 2024. Micro-scale investigations on the mechanical properties of expansive soil subjected to freeze-thaw cycles. *Cold Regions Science and Technology*, 219:104128. https://doi.org/10.1016/j.coldregions.2024.104128

Chen XB, Liu JK, Liu HX, et al., 2006. Frost Action of Soil and Foundation Engineering. Science Press, Beijing, China (in Chinese).

Coussy O, 2006. Deformation and stress from in-pore drying-induced crystallization of salt. *Journal of the Mechanics and Physics of Solids*, 54(8):1517-1547. https://doi.org/10.1016/j.jmps.2006.03.002

Flatt RJ, 2002. Salt damage in porous materials: how high supersaturations are generated. *Journal of Crystal Growth*, 242(3-4):435-454. https://doi.org/10.1016/S0022-0248(02)01429-X

Gao R, 2010. Micro-Macro Degradation Regularity of Sulfate Attack on Concrete under Complex Environments. PhD Thesis, Tsinghua University, Beijing, China (in Chinese).

Jiang L, Niu DT, Yuan LD, et al., 2015. Durability of concrete under sulfate attack exposed to freeze–thaw cycles. *Cold Regions Science and Technology*, 112:112-117. https://doi.org/10.1016/j.coldregions.2014.12.006

Liu Y, Lee FH, Quek ST, et al., 2015. Effect of spatial variation of strength and modulus on the lateral compression response of cement-admixed clay slab. *Géotechnique*, 65(10):851-865. https://doi.org/10.1680/jgeot.14.p.254

Liu Y, Li KQ, Li DQ, et al., 2022. Coupled thermal-hydraulic modeling of artificial ground freezing with uncertainties in pipe inclination and thermal conductivity. *Acta Geotechnica*, 17(1):257-274. https://doi.org/10.1007/s11440-021-01221-w

Mardani-Aghabaglou A, Kalıpcılar İ, Sezer G İ, et al., 2015. Freeze–thaw resistance and chloride-ion penetration of cement-stabilized clay exposed to sulfate attack. *Applied Clay Science*, 115:179-188. https://doi.org/10.1016/j.clay.2015.07.041

MR (Ministry of Railways of the People's Republic of China), 2010. Code for Soil Test of Railway Engineering, TB 10102-2010. National Standards of the People's Republic of China (in Chinese).

Niu DT, Jiang L, Fei QN, 2013. Deterioration mechanism of sulfate attack on concrete under freeze-thaw cycles. *Journal of Wuhan University of Technology-Material Science Edition*, 28(6):1172-1176. https://doi.org/10.1007/s11595-013-0839-6

Puppala AJ, Intharasombat N, Vempati RK, 2005. Experimental studies on ettringite-induced heaving in soils. *Journal of Geotechnical and Geoenvironmental Engineering*, 131(3):325-337. https://doi.org/10.1061/(asce)1090-0241(2005)131:3(325)

Puppala AJ, Congress SSC, Talluri N, et al., 2019. Sulfate-heaving studies on chemically treated sulfate-rich geomaterials. *Journal of Materials in Civil Engineering*, 31(6):04019076. https://doi.org/10.1061/(ASCE)MT.1943-5533.0002729

Qiu GQ, Liu JR, Liu HX, 1994. Geocryological Glossary. Gansu Science and Technology Press, Lanzhou, China (in Chinese).

Ren JG, Lai YM, 2021. Study on the durability and failure mechanism of concrete modified with nanoparticles and polypropylene fiber under freeze-thaw cycles and sulfate attack. *Cold Regions Science and Technology*, 188:103301. https://doi.org/10.1016/j.coldregions.2021.103301

Santhanam M, Cohen MD, Olek J, 2003. Effects of gypsum formation on the performance of cement mortars during external sulfate attack. *Cement and Concrete Research*, 33(3):325-332. https://doi.org/10.1016/S0008-8846(02)00955-9

Sherwood PT, 1962. Effect of sulfates on cement- and lime-stabilized soils. The 41st Annual Meeting of the Highway Research Board, p.98-107.

Slater D, Floyd M, Wimpenny DE, 2003. A summary of the highways agency thaumasite investigation in gloucestershire: the scope of work and main findings. *Cement and Concrete Composites*, 25(8):1067-1076. https://doi.org/10.1016/S0958-9465(03)00131-8

Thaulow N, Sahu S, 2004. Mechanism of concrete deterioration due to salt crystallization. *Materials Characterization*, 53(2-4):123-127. https://doi.org/10.1016/j.matchar.2004.08.013

Wang L, Roy A, Seals RK, et al., 2003. Stabilization of sulfate-containing soil by cementitious mixtures mechanical properties. *Transportation Research Record: Journal of the Transportation Research Board*, 1837(1):12-19. https://doi.org/10.3141/1837-02

Wang PC, Ye YS, Zhang QL, et al., 2020. Investigation on the sulfate attack-induced heave of a ballastless track railway subgrade. *Transportation Geotechnics*, 23:100316. https://doi.org/10.1016/j.trgeo.2020.100316

Wang Q, Liu JK, Wang PC, et al., 2021. Influence of specific surface area on sulfate attack-induced expansion of cement-treated aggregates. *Bulletin of Engineering Geology and the Environment*, 80(6):4841-4854. https://doi.org/10.1007/s10064-021-02200-x

Xiao QH, Cao ZY, Guan X, et al., 2019. Damage to recycled concrete with different aggregate substitution rates from the coupled action of freeze-thaw cycles and sulfate attack. *Construction and Building Materials*, 221:74-83. https://doi.org/10.1016/j.conbuildmat.2019.06.060

Xiao Z, Lai YM, Zhang MY, 2018. Study on the freezing temperature of saline soil. *Acta Geotechnica*, 13(1):195-205. https://doi.org/10.1007/s11440-017-0537-1

Xu F, Wang SL, Li T, et al., 2021. The mechanical properties and resistance against the coupled deterioration of sulfate attack and freeze-thaw cycles of tailing recycled aggregate concrete. *Construction and Building Materials*, 269:121273. https://doi.org/10.1016/j.conbuildmat.2020.121273

Yao JK, Ye YS, Wang PC, et al., 2019. Subgrade heave of sulfate attacking on cement-stabilized filler. *Chinese Journal of Geotechnical Engineering*, 41(4):782-788 (in Chinese). https://doi.org/10.11779/CJGE201904024

Yao YZ, Liu C, Liu HW, et al., 2023. Deterioration mechanism understanding of recycled powder concrete under coupled sulfate attack and freeze-thaw cycles. *Construction and Building Materials*, 388:131718. https://doi.org/10.1016/j.conbuildmat.2023.131718

Zhou Q, Hill J, Byars EA, et al., 2006. The role of pH in thaumasite sulfate attack. *Cement and Concrete Research*, 36(1):160-170. https://doi.org/10.1016/j.cemconres.2005.01.003